Available online at www.sciencedirect.com
ScienceDirect
Journal of Catalysis 244 (2006) 102–112
JOURNAL OF CATALYSIS
www.elsevier.com/locate/jcat

Stabilization of active Rh_2O_3 species for catalytic decomposition of N_2O on La-, Pr-doped CeO_2

A. Bueno-López *, I. Such-Basáñez, C. Salinas-Martínez de Lecea

Inorganic Chemistry Department, University of Alicante, Ap.99 E-03080, Alicante, Spain

Received 21 June 2006; revised 30 August 2006; accepted 30 August 2006

Available online 2 October 2006

Abstract

CeO_2 and La- or Pr-doped CeO_2 were prepared at calcination temperatures of 600, 800, and 1000 °C. The samples were characterized by Raman, XRD, and N_2 adsorption and tested as Rh_2O_3 support for the catalytic decomposition of N_2O at low temperature (starting at 200 °C). Catalyst characterization was done by XPS analysis of fresh and in situ treated catalysts, TPR, and TEM. As deduced by XPS analysis and catalytic tests, Rh_2O_3 is more active than Rh^0 for N_2O decomposition. Pure CeO_2 calcined at low temperature (600 °C) and La or Pr-doped CeO_2 calcined at 600, 800 or 1000 °C can keep Rh_2O_3 stable under reaction conditions. In contrast, Rh_2O_3 supported on pure CeO_2 calcined at high temperature (800 or 1000 °C) is reduced to Rh^0 under reaction conditions. The redox properties of the support are decisive for Rh_2O_3 stabilization and catalytic performance; the larger the reducible surface CeO_2 (determined by TPR), the better the catalytic activity. In addition, structural and textural features of the support (crystallinity, BET surface area, and particle size) affect Rh_2O_3 dispersion, the smaller the support particle size (the higher the surface area), the better the dispersion and the catalytic activity. The redox properties and particle size of supports depend on calcination temperature. Doping improves thermal stability with regard to pure CeO_2. La and Pr form solid solutions with CeO_2, preventing sintering and maintaining a high percentage of reducible CeO_2 at high calcination temperatures (800 and 1000 °C).

Keywords: N_2O decomposition; Rhodium catalyst; Rh_2O_3; Ceria support; Lanthanum; Praseodymium doping; Solid solution; In situ XPS

1. Introduction

Over the last decade, concerns about the N_2O abatement have developed in the scientific community, as reflected in the literature [1–5]. N_2O abatement is attracting attention due to the greenhouse effect contribution and ozone-depleting action of this gas. Anthropogenic sources include adipic acid production, nitric acid manufacture, fossil fuel and biomass combustion, land cultivation, and vehicle emissions [1]. N_2O emissions in gasoline-powered engines have been related to TWC aging, and N_2O is also emitted as byproduct of Pt-based prototypic catalysts for HC-SCR-deNO_x in diesel engine exhausts [6].

Heterogeneous catalytic decomposition is a suitable solution in many of the already mentioned emission sources, and a number of solid catalysts have been proposed, including supported and unsupported metals, pure and mixed oxides, and zeolitic systems [1]. The reported metal catalysts, including Pt, Pd, Ag, Au, and Ge, are generally active above 375 °C, and among the pure oxides, the highest activities are exhibited by the transition metal oxides of group 9 (Rh, Ir, Co, Fe, Ni), CuO and some rare-earth oxides, such as La_2O_3. A comparison of specific activities (per unit surface area) of various pure oxides reveals that Rh_2O_3 produces one of the better results. As noted by Kapteijn et al. [1], supported oxides are not as frequently studied as the pure and mixed oxides, but for practical applications they might be better suited due to their higher dispersion by combination with a high specific surface area support. Often their behavior is compatible with that of the pure oxide, but the loading, method of preparation, and thermal history determine the final catalyst performance, and the distinction between supported oxide and solid solution may vanish.

Catalysts of rhodium dispersed on various supports can be found in the literature [3–5]. In some of them, the catalyst is reduced previous to the catalytic test; however, under reaction

* Corresponding author. Fax: +34 965 90 34 54.
E-mail addresses: agus@ua.es (A. Bueno-López), ion.such@ua.es (I. Such-Basáñez), C.Salinas@ua.es (C. Salinas-Martínez de Lecea).

0021-9517/$ – see front matter
doi:10.1016/j.jcat.2006.08.021

conditions, the rhodium species acting as active centers have not been clearly elucidated. As reported in the literature [1], the reaction of N_2O with the catalyst active centers is generally seen as a charge donation from the catalyst into the antibonding orbitals of N_2O. Metal surface and oxides with more than one valence can act as such centers, but F centers (vacancies in an oxide surface with a trapped electron) also have been proposed for interpreting the activities of oxide surfaces.

Ceria supports are of interest because of their oxygen storage capacity, which strongly affects the oxidation state of the elements that are supported. Martínez-Arias et al. [7] reported a spectroscopic study by ESR and FTIR of active-phase–support interactions on a RhO_x/CeO_2 catalyst and provided evidence of the electronic interactions between RhO_x and CeO_2, which favor the stabilization of cationic species of rhodium on the ceria surface. Fornasiero et al. [8] reported the important role of CeO_2–ZrO_2 in modifying the catalytic activity of supported rhodium for NO reduction by CO.

The decomposition of N_2O over rhodium/CeO_2–ZrO_2 catalysts was studied by Imamura et al. [5], who concluded that ceria is fragile against high-temperature calcination, whereas the addition of Zr significantly increases its thermal stability. Pr-doped CeO_2 has also showed enhanced performance with regard to pure CeO_2 as rhodium support for catalytic decomposition of N_2O [9]. It was concluded that incorporation of Pr to CeO_2 modifies the nature of the lattice oxygen and promotes its removal. This effect leads to improved N_2O reduction activity of the composite oxides when combined with Rh. However, details on the nature of the reducible sites and the function of Pr were not reported.

In fact, it remains unclear how the well-established metal–support interaction in rhodium/CeO_2 catalysts is related to the activity of such catalysts in N_2O decomposition. The objective of this study was to analyze the effect of the ceria properties (particle size, surface area, crystalline structure, and reducibility) in the catalytic activity of supported Rh_2O_3 for N_2O decomposition. Different CeO_2 and La- or Pr-doped CeO_2 supports were prepared, characterized, and used as Rh_2O_3 supports. Catalytic tests under flow conditions were combined with XPS characterization of the rhodium species before and after in situ treatment of the different catalysts under reaction conditions.

2. Experimental

2.1. Catalyst preparation

CeO_2 and 10 wt% La- or Pr-doped CeO_2 supports were prepared from $Ce(NO_3)_3{\cdot}6H_2O$ (Aldrich, 99.9%), $La(NO_3)_3{\cdot}6H_2O$ (Merck, 99.9%), and $Pr(NO_3)_3{\cdot}6H_2O$ (Aldrich, 99.9%). The required amounts of these precursors were mixed in a mortar and calcined in static air at 600, 800, or 1000 °C for 90 min (heating rate, 10 °C/min). The CeO_2-, La-, and Pr-doped CeO_2 supports are denoted by CeO_2T, CeO_2LaT, and CeO_2PrT, respectively, with T being 600, 800, or 1000 depending on the calcination temperature. Supports were further impregnated with $Rh(NO_3)_3$ (Alfa, 99.9%) dissolved in the minimum volume of water, dried at 200 °C, and calcined at 500 °C to form Rh_2O_3 (0.5 wt% Rh target). The nomenclature of the catalysts includes "Rh" before the corresponding support notation.

2.2. Characterization of supports and catalysts

Raman spectra of the supports were recorded in a Bruker RFS 100/S Fourier transform Raman spectrometer with a variable-power Nd:YAG laser source (1064 nm). The laser beam was focused on the sample in a 180° backscattering configuration, and 64 scans at 85 mW laser power (70 mW on the sample) were recorded. No heating of the sample was observed under these conditions.

X-ray diffractograms of the supports were recorded in a Bruker D8 advance diffractometer, using CuK_α radiation ($\lambda = 0.15418$ nm). Spectra were recorded between 10° and 80° (2θ) with a step of 0.02 and a time per step of 3 s. The average crystallite size (D) of supports was determined using the approaches of Scherrer and Williamson–Hall.

In Scherrer's equation,

$$D = \frac{K \cdot \lambda}{\beta \cdot \cos\theta}, \tag{1}$$

where λ is the X-ray wavelength, K is the particle shape factor, taken as 0.94 [10], β was defined as the width at half maximum of the peak and θ is the position (angle) of the peak. Williamson–Hall plots (WH plot) separate the effects of size and strain in the nanocrystals, using the equation

$$\beta_{\text{Total}} = \beta_{\text{Size}} + \beta_{\text{Strain}} = \frac{0.9 \cdot \lambda}{D \cdot \cos\theta} + \frac{4 \cdot (\Delta d) \cdot \sin\theta}{d \cdot \cos\theta},$$

where β_{Total} is the full-width half-maximum of the XRD peak, λ is the incident X-ray wave length, θ is the position of the peaks, D is the crystal size, and Δd is the difference of the d spacing corresponding to a typical peak. A plot of $\beta_{\text{Total}} \cdot \cos\theta$ against $4 \cdot \sin\theta$ yields the crystal size from the intercept value. The BET surface area of the supports was determined by physical adsorption of N_2 at −196 °C in an automatic volumetric system (Autosorb-6, Quantachrome).

A JEOL (JEM-2010) microscope, equipped with an EDS analyzer (OXFORD, model INCA Energy TEM100), was used to obtain the TEM images of the catalysts. A few droplets of an ultrasonically dispersed suspension of each catalyst in ethanol were placed in a cupper grid with lacey carbon film and dried at ambient conditions for TEM characterization.

Temperature-programmed reduction (TPR) of the catalysts was carried out in a Micromeritics Pulse ChemiSorb 2705 device, consisting of a tubular quartz reactor (5 mm i.d.) coupled to a TCD analyzer to monitor H_2 consumption. The experiments were conducted with 20 mg of fresh catalyst at a ramp rate of 10 °C/min from room temperature to 900 °C in 30 ml/min flow of 5 vol% H_2 in Ar. To quantify the total amount of H_2 consumed, CuO was used as calibration reference.

XPS characterization of selected catalysts was carried out in a VG-Microtech Multilab electron spectrometer using a MgK_α (1253.6 eV) radiation source. To obtain the XPS spectra, the pressure of the analysis chamber was maintained at

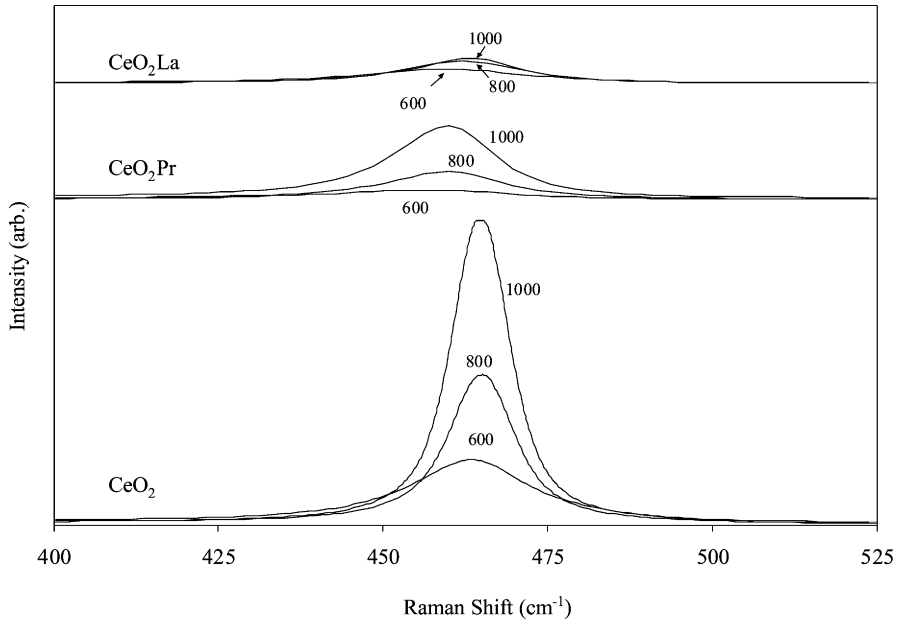

Fig. 1. Raman spectra of the supports.

5×10^{-10} mbar. The binding energy (BE) and the kinetic energy (KE) scales were adjusted by setting the C 1s transition at 284.6 eV, and BE and KE values were determined with the Peak-fit software of the spectrometer. XPS spectra were recorded for fresh and in situ treated catalysts under N_2O at 225 °C for 1 h. The in situ treatment was carried out before the XPS measurement in an auxiliary reaction chamber, where the sample was heated to the preselected temperature and the gas mixture (1000 ppm N_2O/He, 1 atm total pressure) was fed. After the treatment, the sample was introduced into the XPS chamber, avoiding exposure to air.

2.3. N_2O decomposition tests

N_2O decomposition tests were performed in a cylindrical, fixed-bed, 10-mm-i.d. reactor at atmospheric pressure, using 50 mg of catalyst diluted with 350 mg of CSi and a total flow rate of 100 ml/min (1000 ppm N_2O/He; GHSV = 12,000 h^{-1}). The experiments consisted of point-by-point isothermal reactions in the range of 100–500 °C, which were extended until steady state was reached. The gas composition was analyzed using a HP 6890 gas chromatograph equipped with a thermal conductivity detector and two serial columns (Porapak Q, used for N_2O monitoring, and Molecular Sieve 13X, for O_2 and N_2 separation).

3. Results and discussion

3.1. Characterization of supports

Materials based on ceria show a Raman characteristic main band at about 465 cm^{-1} assigned to the mode F_{2g} of fluorite-type structures [10,11], as shown in Fig. 1. The Raman spectrum of ceria is dominated by oxygen lattice vibrations and is sensitive to the crystallinity of the sample [12]. An increase in calcination temperature produces a significant increase in the intensity of the F_{2g} band, and thus an increase in the crystallinity of the material can be inferred as the calcination temperature rises. The spectra in Fig. 1 corresponding to CeO_2La*T* and CeO_2Pr*T* supports do not show evidence of La_2O_3 [13] or any other species of La or Pr, suggesting that La and Pr are located in the CeO_2 lattice forming solid solutions. The presence of dopants, such as La or Pr, in the CeO_2 lattice has been reported to cause deformation of the fluorite-type structure, thereby decreasing the intensity of the 465 cm^{-1} band [14] and in some cases shifting the position of the F_{2g} peak [15–17] slightly, in accordance to the results observed in Fig. 1.

Powder X-ray diffractograms of the supports are shown in Fig. 2. These contain only the main reflections typical of a fluorite-structured material with an fcc unit cell, corresponding to the (111), (200), (220), (311), (222), and (400) planes [18]. As calcination temperature increases, the peaks narrow, related to increased crystal size. X-ray diffraction patterns confirm that La- and Pr-containing supports present the true mixed-oxide phase with the cubic fluorite-type structure typical of CeO_2. La_2O_3 characteristic peaks [13] are not observed in the diffractograms, confirming that segregation of phases does not occur in La-doped CeO_2 supports. In Pr-containing CeO_2, Raman spectra suggest that Pr is located in the CeO_2 framework and Pr^{3+} is expected according to the numerous oxygen vacancies detected in Ce–Pr–O samples as reported previously [14].

Note that although La shifts the characteristic CeO_2 peaks slightly to lower angles, adding Pr does not change the peak positions significantly. This suggests that La-doped samples sustain an expansion of the lattice parameter of the unit cell [15–17] due to the larger ionic radii of La^{3+} (1.16 Å) compared with Ce^{4+} (0.97 Å). As reported previously, adding La to a CeO_2 lattice could result in a lattice expansion that amounts to approximately 0.5% expansion for a sample doped with 10% of La [19]. However, in the case of Pr, peak positions do not

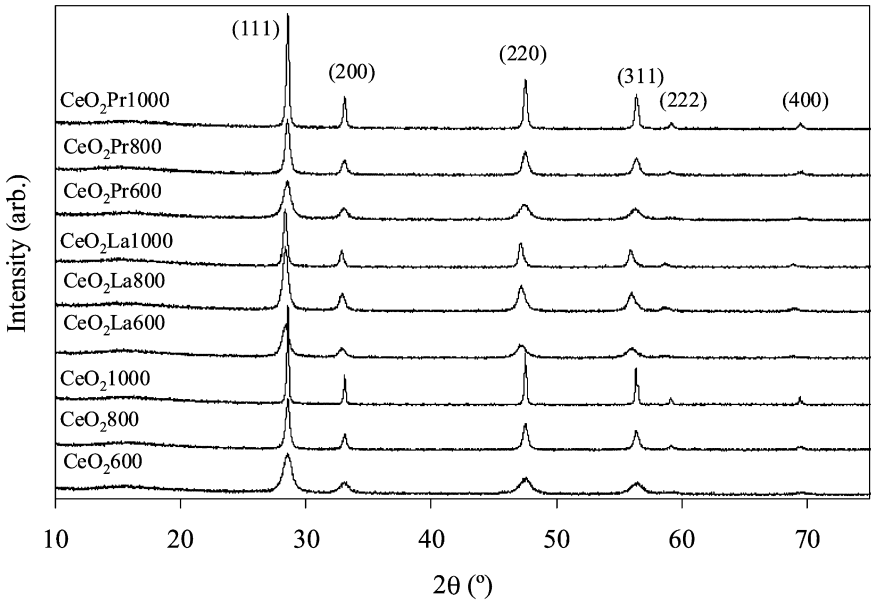

Fig. 2. XRD patterns of the supports.

Table 1
Supports properties

Support	Particle size Scherrer (nm)	Particle size WH plot (nm)	BET (m^2/g)
$CeO_2$600	11	13	76
$CeO_2$800	23	25	26
$CeO_2$1000	43	66	6
CeO_2La600	14	20	49
CeO_2La800	17	26	37
CeO_2La1000	26	33	17
CeO_2Pr600	13	17	44
CeO_2Pr800	20	21	30
CeO_2Pr1000	36	46	13

reveal significant lattice expansion, consistent with the similar size of Ce^{4+}/Ce^{3+} and Pr^{4+}/Pr^{3+} cations (0.97/1.14 and 0.96/1.13 Å, respectively).

The average crystallite sizes of the supports determined using Scherrer's equation and the WH plot are compiled in Table 1. Increasing the calcination temperature increases crystal size. However, when doping ceria with La or Pr, this effect is mitigated, as observed previously for Pr [9]. He et al. [20] reported that the average crystallite size decreases by doping CeO_2–ZrO_2 solid solutions with Y^{3+} cations, as also occurs at 800 °C and 1000 °C when CeO_2 is doped with either La or Pr. BET surface area (reported in Table 1) also reflects particle size growth with increasing calcination temperature.

3.2. Catalyst characterization by TEM

TEM pictures of the catalysts are compiled in Fig. 3, showing that both the calcination temperature and La or Pr doping of the support affect catalyst appearance. Increasing support calcination temperature resulted in a larger particle size. Individual crystals are hardly observed in the TEM pictures of the three catalysts with supports calcined at 600 °C. According to XRD results (WH plot calculations), the average crystal size of the 600 °C-calcined supports is about 13–20 nm. In contrast, well-defined crystals of CeO_2 are observed in catalysts prepared with supports calcined at 800 and 1000 °C, and the observed sizes are very consistent with those obtained from XRD. Crystals of around 20–25 nm are observed in supports calcined at 800 °C, and even larger crystals are seen in those catalysts prepared on supports calcined at 1000 °C. $RhCeO_2La1000$ has the smallest support particle size among those prepared at 1000 °C (33 nm, according to the W-H plot), compared with $RhCeO_2Pr1000$ (46 nm) and $RhCeO_21000$ (66 nm).

Rh_2O_3 particles were clearly identified in TEM images of catalysts $RhCeO_2800$, $RhCeO_21000$, and $RhCeO_2Pr1000$ by in situ EDS microanalysis, as shown in Fig. 4, and the Rh_2O_3 crystal size was roughly estimated as <3 nm. Individual particles of Rh_2O_3 were observed in the TEM pictures of $RhCeO_2800$ and $RhCeO_2Pr1000$, whereas the micrograph of $RhCeO_21000$ showed that in this case, Rh_2O_3 particles were not individually dispersed on the surface of the support but rather formed aggregates. Imamura et al. [5] also observed that rhodium was present in an aggregate state on CeO_2/ZrO_2 supports calcined at high temperature (1200 °C), and deduced that rhodium present in this state had low catalytic activity for N_2O decomposition despite its high surface concentration.

In the rest of the samples, Rh_2O_3 particles were not observed by TEM. This is evidence of the high dispersion. From these results, it can be deduced that the low crystallinity and small particle size observed on Raman and XRD favor high dispersion of rhodium species.

3.3. Catalyst characterization TPR

H_2 consumption profiles during the TPR experiments are plotted in Fig. 5. Considering the composition of the sam-

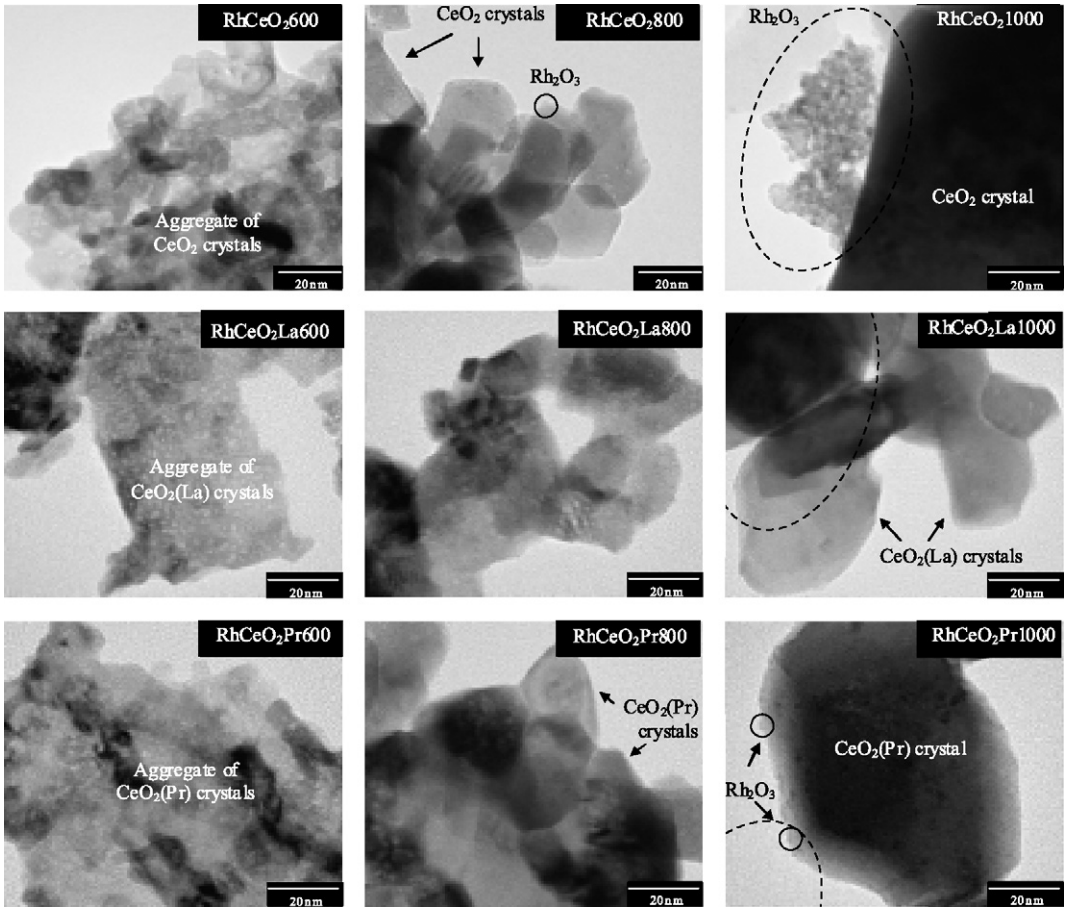

Fig. 3. TEM pictures of the different catalysts. (The dashed lines included in the pictures of $RhCeO_2$1000, $RhCeO_2$La1000 and $RhCeO_2$Pr1000 indicate the areas selected for local EDS analysis.)

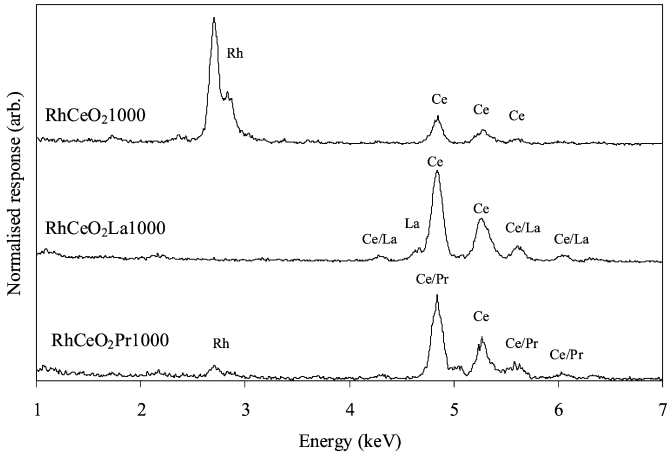

Fig. 4. Local EDS analysis of TEM pictures. (The analysed areas are indicated in Fig. 3 by dashed lines.)

ples, H_2 consumption can be attributed to two main chemical processes, as follows:

- Rh_2O_3 reduction to metallic Rh^0, according to the reaction
$$Rh_2O_3 + 3H_2 \rightarrow 2Rh + 3H_2O. \quad (2)$$
- CeO_2 reduction to Ce_2O_3, according to the reaction
$$2CeO_2 + H_2 \rightarrow Ce_2O_3 + H_2O. \quad (3)$$

Other phenomena also must be considered. The carbon monoxide and carbon dioxide desorbing from the sample due to carbonates occluded at the surface or in the structure can also reach the thermally controlled detector and contribute to the variations in conductivity of the actual reduction mixture, as reported previously [21]. Pr-containing samples could also consume H_2 due to the reduction of Pr^{4+} to Pr^{3+}. This does not occur in the La-containing samples, however, because 3+ is the only oxidation state of lanthanum allowed.

Three peaks are shown for most of the samples in Fig. 5, in agreement with TPR profiles described in the literature for similar materials, such as Rh/CeO_2 and $Rh/Pr–CeO_2$ [9]; Rh-loaded $CeO_2–ZrO_2$ solid solutions [22]; Pd-, Pt-, and Rh-loaded $Ce_{0.5}Zr_{0.5}O_2$ [23]; and Pd-, Pt-, and Rh-loaded $Ce_{0.6}Zr_{0.35}Y_{0.05}O_2$ [24].

The first peak in $RhCeO_2$1000 corresponds to the reduction of Rh_2O_3, and in the rest of the samples also includes CeO_2 reduction (via reaction (3)) because the ratio H_2/Rh is greater than the stoichiometric for reaction (2). It is generally accepted that the reduction of CeO_2 occurring in the first peak occurs at the surface of the support particles and that the peak at highest temperature is attributed to bulk CeO_2 reduction (reaction (3)) [22]. There is no agreement in the literature regarding the second peak detected in the TPR patterns; some authors attribute it to surface ceria reduction as well [22], whereas others link it to

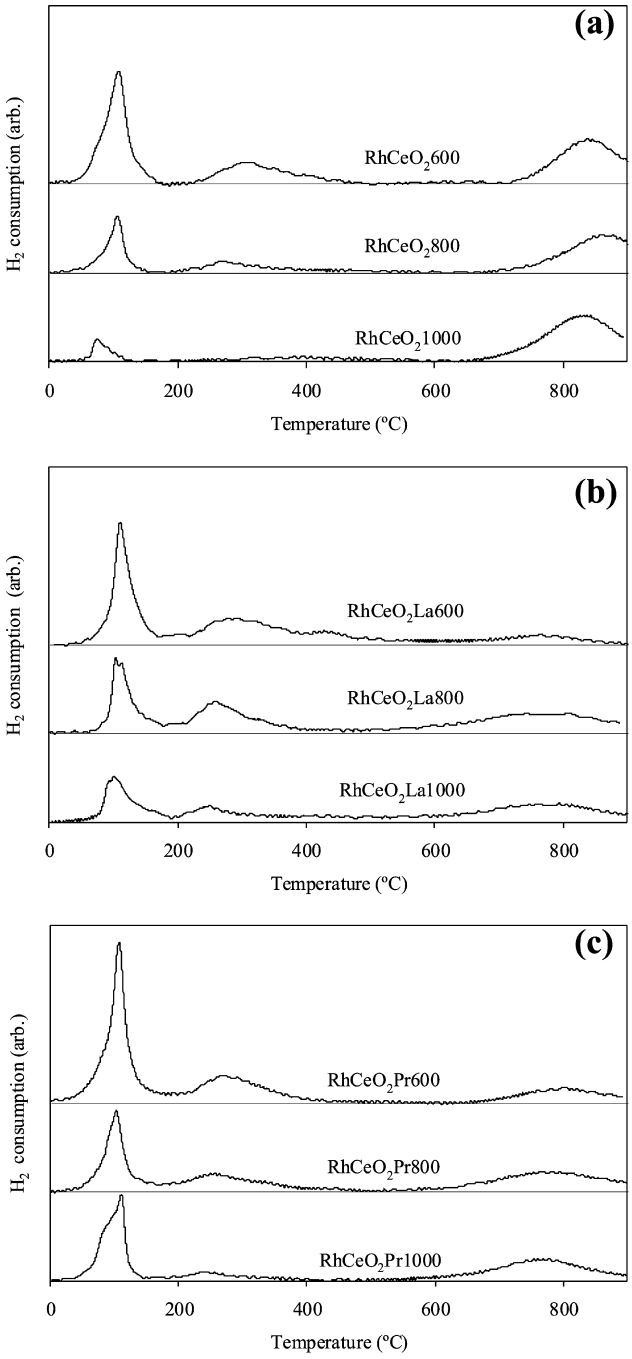

Fig. 5. H_2 consumption profiles during TPR for catalysts containing (a) CeO_2 supports, (b) CeO_2La supports, and (c) CeO_2Pr supports.

decomposition of carbonates occluded at the surface or in the structure of the ceria [21].

The absence of surface CeO_2 reduction in $RhCeO_21000$ is reasonable because the surface area of the support of this sample is very low (BET = 6 m^2/g). In contrast, the amount of H_2 consumed in the first peak by $RhCeO_2800$ and $RhCeO_2600$ (Fig. 5a) is much higher than that expected from the stoichiometry of Eq. (2), indicating that surface CeO_2 reduction occurred along with Rh_2O_3 reduction. Similar behavior is seen for the La- and Pr-containing catalysts, regardless of the calcination temperature of the support.

Table 2
Surface Ce^{4+} reduced to Ce^{3+} in TPR experiments

Catalyst	$Ce^{4+}_{reduced}/Ce_{total}$ (%)		Monolayers CeO_2 reduced	
	First peak	Second peak	First peak	Second peak
$RhCeO_2600$	10.6	6.4	0.46	0.28
$RhCeO_2800$	3.1	3.5	0.39	0.44
$RhCeO_21000$	0.0	0.0	0.00	0.00
$RhCeO_2La600$	10.8	11.8	0.65	0.71
$RhCeO_2La800$	6.5	9.5	0.51	0.75
$RhCeO_2La1000$	4.8	5.9	0.84	1.03
$RhCeO_2Pr600$	13.6	8.3	1.01	0.62
$RhCeO_2Pr800$	7.2	6.5	0.78	0.70
$RhCeO_2Pr1000$	6.7	2.6	1.12	0.44

The percentages of Ce^{4+} reduced to Ce^{3+} were determined considering the amounts of H_2 consumed during the experiments and the stoichiometry of Eq. (3), and are given in Table 2. For these calculations, the first and second peaks observed in Fig. 5 were considered, and the amount of H_2 necessary to reduce completely Rh_2O_3 to Rh^0 was subtracted from the amount of H_2 consumed in the first peak. In addition, the number of reacted monolayers of CeO_2 has been estimated by assuming that CeO_2 has an average of 13.1 surface oxygen atoms/nm^2 and the BET surface area, as reported previously [25].

As observed in Table 2, the number of monolayers of CeO_2 reduced in the first peak is near or below 1, indicating that surface CeO_2 is partially or completely reduced and confirming that bulk reduction has not taken place at this range of temperatures. Considering both the first and second peaks, the number of monolayers of CeO_2 reduced is >1 for all of the samples with doped CeO_2, indicating that not only the surface is reduced. This could be related to the decomposition of carbonates occluded at the surface or in the structure of the ceria, as reported previously [21], and/or to the reduction of CeO_2 located below the surface. Considering this, only the CeO_2 reduced in the first peak is considered as surface CeO_2 reduced for further calculations.

The percentage of surface Ce^{4+} reduced in the first peak decreases with the calcination temperature of the support. This phenomenon is more important in CeO_2 than in La- or Pr-doped CeO_2. This decrease is in agreement with the decrease in BET surface area of the support. For samples calcined at similar temperatures, surface reduction is greater in doped CeO_2 than in pure CeO_2, indicating that La and Pr doping improves the redox properties of CeO_2. Fig. 6 plots the percentage of surface CeO_2 reduced against the BET surface area of the support, showing a linear relationship for the catalysts prepared with pure CeO_2. However, improved redox properties are seen for La- and Pr-doped CeO_2 in comparison to pure CeO_2; that is, for similar BET surface areas, the amount of surface CeO_2 reduced is greater in La- or Pr-doped samples than in pure CeO_2, and Pr doping seems to be more effective than La doping.

3.4. N_2O decomposition tests

Fig. 7 plots the N_2O conversion percentage as a function of the reaction temperature for catalysts with supports calcined

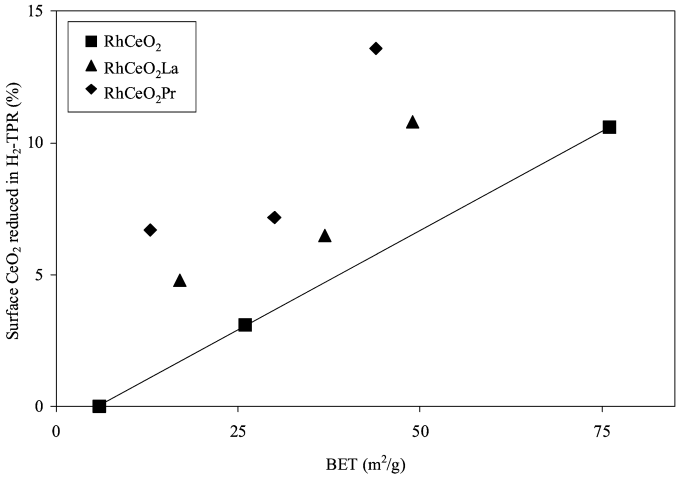

Fig. 6. Surface CeO_2 reduced in TPR versus BET surface area.

at 600 °C (Fig. 7a), 800 °C (Fig. 7b), and 1000 °C (Fig. 7c). All of the catalysts shown in Fig. 7a are highly active for N_2O decomposition, with the temperature at onset of N_2O decomposition as low as 200 °C and that of complete N_2O conversion at 300 °C. Note that the CeO_2La600 support shows no activity for N_2O decomposition below 300 °C, indicating that in the temperature range where rhodium species are active, the supports themselves are not able to decompose N_2O. However, considering the different curves shown in Fig. 7, a considerable effect of the support is observed. Among the catalysts compared in Fig. 7a, $RhCeO_2La600$ and $RhCeO_2Pr600$ show slightly higher activity than $RhCeO_2600$. The differences in the activity of catalysts shown in Fig. 7c are much more important than those shown in Fig. 7a. $RhCeO_21000$ activity is delayed to temperatures above 300 °C, whereas $RhCeO_2La1000$ and $RhCeO_2Pr1000$ maintain their activity at about 200 °C. The behavior of catalysts with supports treated at 800 °C is intermediate. Again, $RhCeO_2800$ is less active than those catalysts with doped CeO_2 supports.

From these experiments, it can be concluded that the decomposition of N_2O over Rh_2O_3 catalysts is strongly affected by the properties of the support used, with La- or Pr-doped CeO_2 more effective than pure CeO_2. The calcination temperature of the support strongly affects pure CeO_2, but this effect is not very important in La- or Pr-doped CeO_2.

To analyze the properties of the supports affecting the catalytic activity of Rh_2O_3, the percentage of N_2O decomposed at 225 °C versus the surface area of the support is plotted in Fig. 8. A linear relationship is obtained, which is reasonable because the dispersion of Rh_2O_3 is enhanced by increasing the support surface area. This is in agreement with the TEM pictures (Fig. 3), where Rh_2O_3 particles are observed only over supports with large particle sizes and, consequently, low surface area. However, the relationships in Fig. 8 are different for ceria and doped ceria catalysts. Considering supports with similar surface area, the catalysts with La- or Pr-doped CeO_2 supports are more effective for N_2O decomposition. This indicates that the surface area is not the unique characteristic of the support affecting Rh_2O_3 activity. The redox properties of the support, which are modified by La and Pr doping, could be the other property affecting catalytic activity of Rh_2O_3. This can be clearly seen in Fig. 9, which plots the catalytic activity versus the reduced surface CeO_2 (determined from TPR). A relationship between reduced surface CeO_2 and N_2O conversion is observed, indicating that N_2O decomposition is also affected by the redox properties of the support.

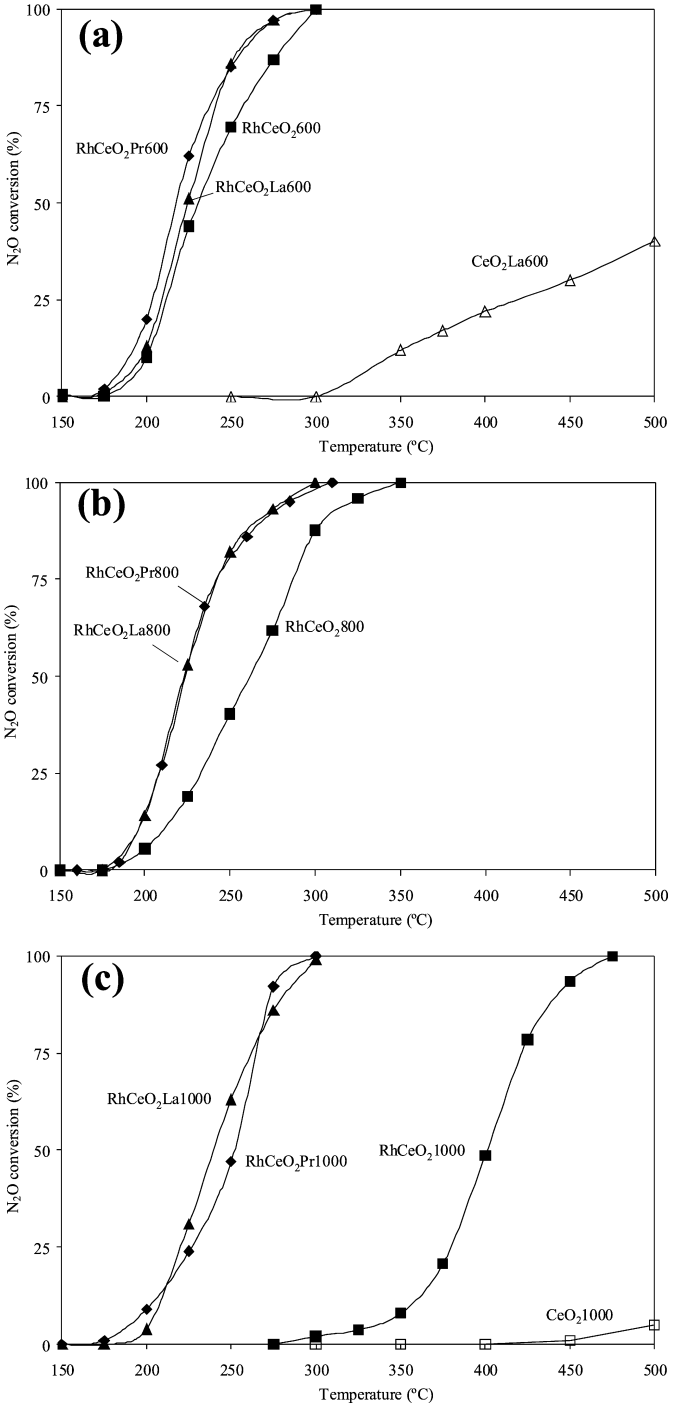

Fig. 7. N_2O conversion as a function of temperature for catalysts with supports calcined at (a) 600, (b) 800, and (c) 1000 °C.

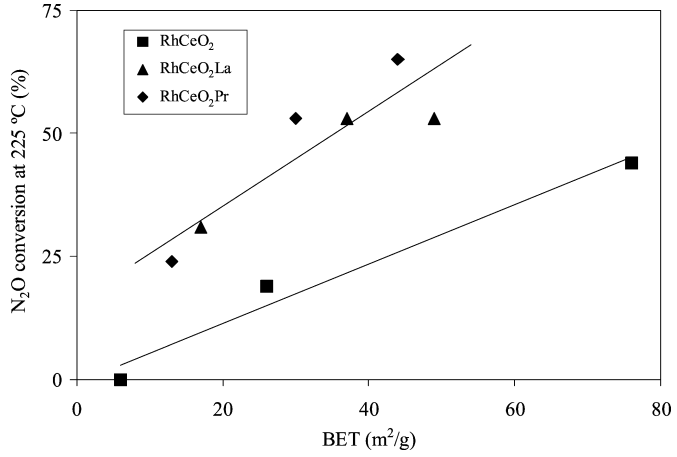

Fig. 8. N_2O conversion at 225 °C versus support BET surface area.

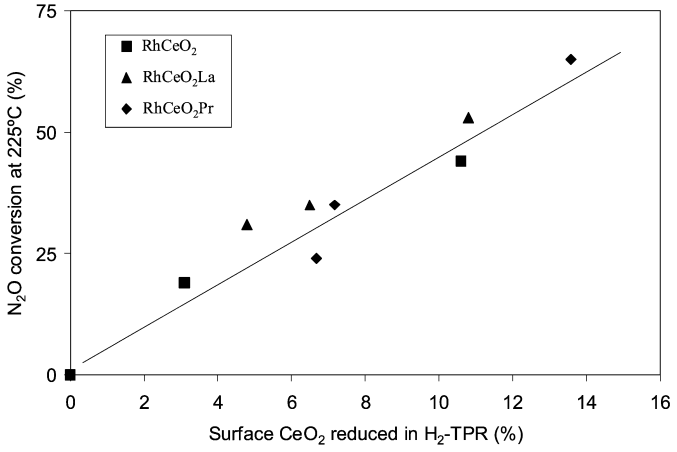

Fig. 9. N_2O conversion at 225 °C versus the surface CeO_2 reduced obtained from TPR.

3.5. Characterization by "in situ" XPS

Rh 3d photoelectron spectra of selected catalysts before and after in situ treatment under N_2O/225 °C are shown in Fig. 10. The Rh $3d_{5/2}$ peak has been reported to appear at 307.0–307.5 eV [26–28] for Rh^0, at about 308.1 eV for Rh(I) [28], and at 308.3–310.5 eV for Rh(III) [26,28]. In addition, another peak appears at higher binding energies attributed to Rh $3d_{3/2}$.

The position of the Rh $3d_{5/2}$ peak for the fresh catalysts tested is 308.6–309.1 eV (Fig. 10a), confirming that the oxidation state of rhodium is 3+, corresponding to Rh_2O_3. This is as expected, because catalysts were calcined to decompose the rhodium precursor. After the in situ treatment under N_2O/225 °C, partial or total Rh_2O_3 reduction is observed in some catalysts. The catalyst $RhCeO_2$600 shows a doublet $3d_{5/2}$ peak with maximum binding energies at 307.2 and 308.8 eV, indicating the presence of Rh^0 and Rh^{3+}, respectively. The percentages of Rh^0 and Rh^{3+} are 50% for each rhodium species, determined by peak deconvolution analysis. A similar situation is observed in $RhCeO_2$800, but in this case, the percentages of Rh^0 and Rh^{3+} are 86% and 14%, respectively. In contrast, 100% Rh^0 is identified in $RhCeO_2$1000, whereas $RhCeO_2$La1000 and $RhCeO_2$Pr1000 contain Rh^{3+} only after the treatment.

This information allows us to conclude that Rh_2O_3 species is more active in the decomposition of N_2O than Rh^0 species. This assumption arises from the fact that more active catalysts (La- and Pr-doped CeO_2) show exclusively a Rh^{3+} signal in XPS spectra, whereas less active catalysts ($RhCeO_2$800 and $RhCeO_2$1000) show Rh^{3+} and/or Rh^0 signals when treated in situ with N_2O/225 °C. The stability of Rh_2O_3 under reaction conditions depends on the properties of the support, and La- or Pr-doped CeO_2 is much more effective than pure CeO_2 in maintaining the stability of Rh_2O_3. As discussed previously, the stabilizing effect of the different supports tested depends on their crystallinity, BET surface area, and particle size, which allows better dispersion of the noble metal on its surface. However, the stabilization of Rh_2O_3 under reaction conditions cannot be explained solely by structural and textural features of the supports (crystallinity, BET surface area, and particle size), because, as shown in Fig. 8, samples with similar BET surface areas (compare, e.g., pure and doped CeO_2) have different activities for N_2O decomposition. As demonstrated, La and Pr also improve the redox properties of CeO_2, increasing the amount of surface CeO_2 reduced in TPR experiments (compare, e.g., samples with similar BET surface areas in Fig. 6). The redox properties of the support strongly affect the activity of catalysts (see Fig. 9), and this improvement may be related to the stabilization of Rh_2O_3 under reaction conditions, avoiding Rh_2O_3 reduction to Rh^0.

Finally, the Ce 3d core level was analyzed; Fig. 11 compares the spectra before (Fig. 11a) and after (Fig. 11b) in situ treatment under N_2O/225 °C. The degree of ceria reduction can be calculated after deconvolution of the experimental spectra, from the ratio of the sum of the intensities of the u_0, u_1, v_0, and v_1 bands to the sum of the intensities of all of the bands [29]. The calculated values are given in Table 3. Most of the fresh catalysts present values around 32–35%; only the Pr-containing sample contains less Ce^{3+} (25.8%). Praseodymium can form 3+ and 4+ cations, and, according to XPS calculations (Pr spectra not shown), 44,6% of praseodymium is 3+, compensating for the lower value of Ce^{3+} with regard to pure CeO_2 or La-doped samples.

After the reaction with N_2O at 225 °C, the $RhCeO_2$1000 support is partially reduced, increasing the percentage of Ce^{3+}. In contrast, the ratio Ce^{3+}/Ce^{4+} in $RhCeO_2$600, $RhCeO_2$800, and $RhCeO_2$La1000 does not change significantly (sample $RhCeO_2$Pr1000 is even slightly oxidized); that is, supports are stable under reaction conditions.

These results confirm the important role of the redox properties of the support in N_2O decomposition. Supports with poor redox properties are partially reduced under reaction conditions, and Rh_2O_3 is also reduced with the corresponding decay in activity. In contrast, supports with improved redox properties are stable under reaction conditions and also are able to stabilize Rh_2O_3. This suggests that N_2O decomposition follows a redox mechanism, first reducing Rh_2O_3 and/or the CeO_2 support. Depending on the redox properties of the support, Rh_2O_3 and/or CeO_2 is or is not reoxidized afterward, and supports with

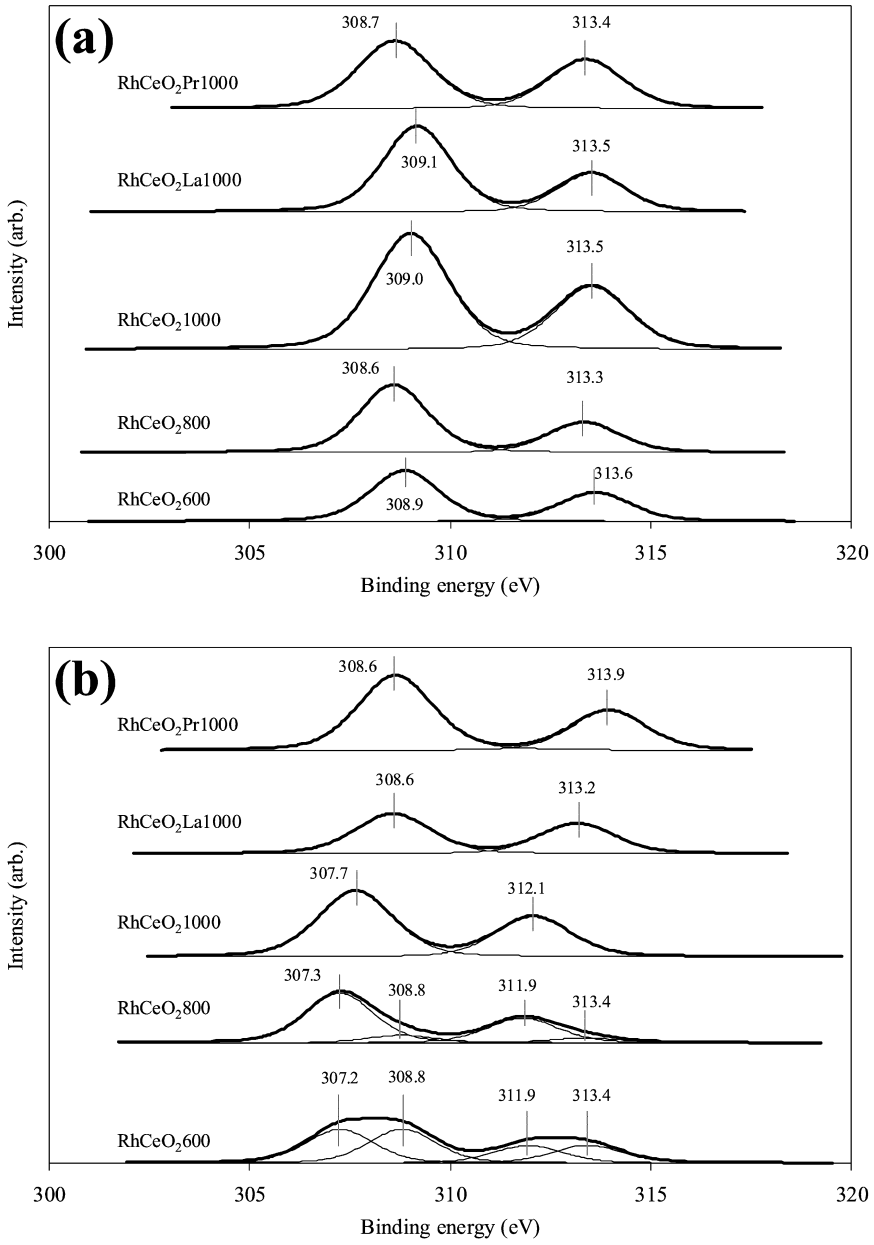

Fig. 10. Rh 3d photoelectron spectra of (a) fresh catalysts and (b) catalysts after an in situ treatment under reaction conditions (N_2O/225 °C).

Table 3
Ce^{3+} percentage on samples before and after reaction with N_2O at 225 °C (determined by XPS)

	Fresh sample	After N_2O/225 °C
$RhCeO_2$600	35.8	36.1
$RhCeO_2$800	35.2	35.2
$RhCeO_2$1000	32.0	35.2
$RhCeO_2$La1000	32.3	31.2
$RhCeO_2$Pr1000	25.8	23.2

improved redox properties are expected to be reoxidized more easily. The oxygen storage capacity of CeO_2 via the Ce^{3+}/Ce^{4+} cycle is well known, and is reasonable to assume that CeO_2 with improved redox properties can provide oxygen to Rh_2O_3 when reduced much better than CeO_2 with poor redox properties.

4. Conclusions

Rh_2O_3/CeO_2 catalysts are active for N_2O decomposition at low temperature (200–300 °C), and CeO_2 supports play a major role in the activity of these catalysts, despite the fact that Rh_2O_3-free supports are not active for N_2O decomposition in this temperature range. Rh_2O_3 is more active than Rh^0 for N_2O decomposition, and the properties of CeO_2 strongly affect the stability of Rh_2O_3 under reaction conditions. Suitable supports are pure CeO_2 calcined at low temperature (600 °C) and La- or Pr-doped CeO_2 calcined at 600, 800, or 1000 °C, because they are able to keep Rh_2O_3 stable under reaction conditions due to metal oxide–support interaction. Otherwise, Rh_2O_3 is reduced to Rh^0, as in the case of Rh_2O_3 supported on pure CeO_2 calcined at 800 or 1000 °C.

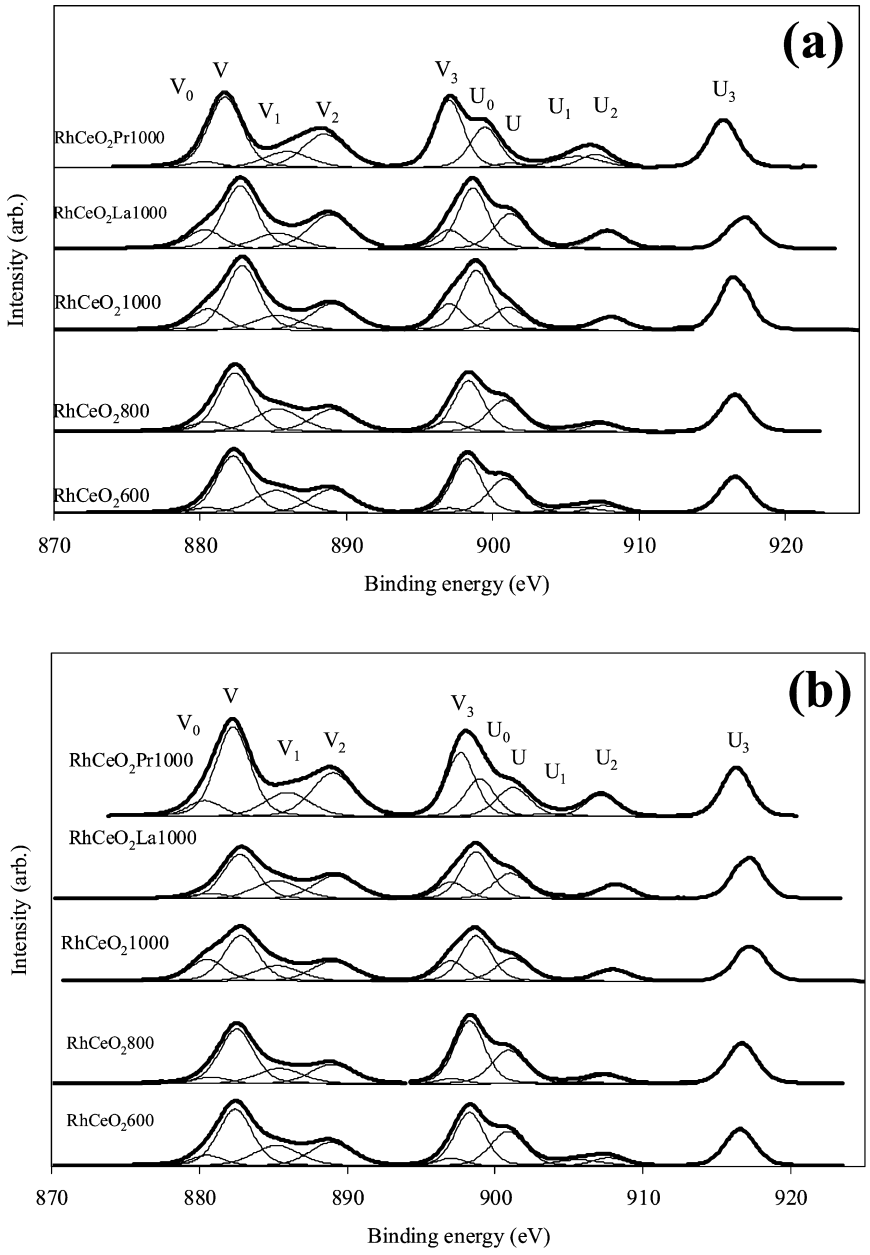

Fig. 11. Ce 3d photoelectron spectra of (a) fresh catalysts and (b) catalysts after an in situ treatment under reaction conditions (N_2O/225 °C).

The redox properties of the support are decisive for Rh_2O_3 stabilization under reaction conditions; the larger the amount of reducible CeO_2 at the surface, the better the catalytic activity. In addition, structural and textural features of the support (crystallinity, BET surface area, and particle size) affect the dispersion of the noble metal; the lower the particle size (i.e., the higher the surface area), the better the catalytic activity.

The redox properties of CeO_2 depend on calcination temperature, and La and Pr doping form solid solutions, leading to higher percentages of reducible surface CeO_2. The particle size of the supports also depends on the calcination temperature. All of the supports show similar particle size when calcined at 600 °C (13–20 nm); however, the presence of La and Pr in CeO_2 supports prevents sintering at higher calcination temperatures.

Acknowledgments

This work was supported by the Spanish Ministry of Education and Science (project MAT2006-12635).

References

[1] F. Kapteijn, J. Rodríguez-Mirasol, J.A. Moulijn, Appl. Catal. B Environ. 9 (1996) 25.
[2] J. Pérez-Ramírez, F. Kapteijn, K. Schoffel, J.A. Moulijn, Appl. Catal. B Environ. 44 (2003) 117.
[3] K. Yuzaki, T. Yarimizu, K. Aoyagi, S. Ito, K. Kunimori, Catal. Today 45 (1998) 129.
[4] G. Centi, S. Perathoner, F. Vazzana, M. Marella, M. Tomaselli, M. Mantegazza, Adv. Environ. Res. 4 (2000) 325.
[5] S. Imamura, R. Hamada, Y. Saito, K. Hashimoto, H. Jindai, J. Mol. Catal. A Chem. 139 (1999) 55.

[6] A. Bueno-López, D. Lozano-Castello, I. Such-Basáñez, J.M. García-Cortés, M.J. Illán-Gómez, C. Salinas-Martínez de Lecea, Appl. Catal. B Environ. 58 (2005) 1.
[7] A. Martínez-Arias, J. Soria, J.C. Conesa, J. Catal. 168 (1997) 364.
[8] P. Fornasiero, G.R. Rao, J. Kaspar, F. L'Erario, M. Graziani, J. Catal. 175 (1998) 269.
[9] S. Imamura, J. Tadani, Y. Saito, Y. Okamoto, H. Jindai, C. Kaito, Appl. Catal. A Gen. 201 (2000) 121.
[10] L.N. Ikryannikova, A.A. Aksenov, G.L. Markaryan, G.P. Murav'eva, B.G. Kostyuk, A.N. Kharlanov, E.V. Lunina, Appl. Catal. A Gen. 210 (2001) 225.
[11] A. Mineshige, T. Taji, Y. Muroi, M. Kobune, S. Fujii, N. Nishi, M. Inaba, Z. Ogumi, Solid State Ionics 135 (2000) 481.
[12] M. Fernández-García, A. Martínez-Arias, A. Iglesias-Juez, C. Belver, A.B. Hungria, J.C. Conesa, J. Soria, J. Catal. 194 (2000) 385.
[13] A. Bueno-López, K. Krishna, M. Makkee, J.A. Moulijn, J. Catal. 230 (2005) 237.
[14] J.R. McBride, K.C. Hass, B.D. Poindexter, W.H. Weber, J. Appl. Phys. 76 (1994) 2435.
[15] J.E. Spanier, R.D. Robinson, F. Zheng, S.W. Chan, I.P. Herman, Phys. Rev. 64 (2001).
[16] F. Zhang, S.W. Chan, J.E. Spanier, E. Apak, Q. Jin, R.D. Robinson, I.P. Herman, Appl. Phys. Lett. 80 (2002) 127.
[17] S. Rossignol, C. Descorme, C. Kappenstein, D. Duprez, J. Mater. Chem. 11 (2001) 2587.
[18] D. Terribile, A. Trovarelli, J. Llorca, C. de Leitenburg, G. Dolcetti, Catal. Today 43 (1998) 79.
[19] K.M. Ryan, J.P. McGrath, R.A. Farrell, W.M. O'Neill, C.J. Barnes, M.A. Morris, J. Phys. Condens. Matter 15 (2003) L49.
[20] H. He, H.X. Dai, K.W. Wong, C.T. Au, Appl. Catal. A Gen. 251 (2003) 61.
[21] F.M.Z. Zotin, L. Tournayan, J. Varloud, V. Perrichon, R. Frety, Appl. Catal. A Gen. 98 (1993) 99.
[22] P. Fornasiero, R. DiMonte, G.R. Rao, J. Kaspar, S. Meriani, A. Trovarelli, M. Graziani, J. Catal. 151 (1995) 168.
[23] P. Fornasiero, J. Kaspar, V. Sergo, M. Graziani, J. Catal. 182 (1999) 56.
[24] H. He, H.X. Dai, L.H. Ng, K.W. Wong, C.T. Au, J. Catal. 206 (2002) 1.
[25] Y. Madier, C. Descorme, A.M. Le Govic, D. Duprez, J. Phys. Chem. B 103 (1999) 103, 10999.
[26] http://www.lasurface.com/.
[27] X.D. Wu, L.H. Xu, D. Weng, Appl. Surf. Sci. 221 (2004) 375.
[28] J. Soria, A. Martínez-Arias, J.L.G. Fierro, J.C. Conesa, Vacuum 46 (1995) 1201.
[29] A. Laachir, V. Perrichon, A. Badri, J. Lamotte, E. Catherine, J.C. Lavalley, J. El Fallal, L. Hilaire, F. le Normand, E. Quéméré, G.N. Sauvion, O. Touret, J. Chem. Soc. Faraday Trans. 87 (1991) 1601.